JOURNAL OF VIROLOGY, Mar. 2004, p. 2935–2942 Vol. 78, No. 6
0022-538X/04/$08.00+0 DOI: 10.1128/JVI.78.6.2935–2942.2004

Cryoelectron Microscopy Analysis of the Structural Changes Associated with Human Rhinovirus Type 14 Uncoating

Elizabeth A. Hewat[1]* and Dieter Blaas[2]

Institut de Biologie Structurale Jean-Pierre Ebel, 38027 Grenoble, France,[1] and Max F. Perutz Laboratories, University Departments at the Vienna Biocenter, Department of Medical Biochemistry, University of Vienna, A-1030 Vienna, Austria[2]

Received 19 August 2003/Accepted 12 November 2003

Release of the human rhinovirus (HRV) genome into the cytoplasm of the cell involves a concerted structural modification of the viral capsid. The intracellular adhesion molecule 1 (ICAM-1) cellular receptor of the major-group HRVs and the low-density lipoprotein (LDL) receptor of the minor-group HRVs have different nonoverlapping binding sites. While ICAM-1 binding catalyzes uncoating, LDL receptor binding does not. Uncoating of minor-group HRVs is initiated by the low pH of late endosomes. We have studied the conformational changes concomitant with uncoating in the major-group HRV14 and compared them with previous results for the minor-group HRV2. The structure of empty HRV14 was determined by cryoelectron microscopy, and the atomic structure of native HRV14 was used to examine the conformational changes of the capsid and its constituent viral proteins. For both HRV2 and HRV14, the transformation from full to empty capsid involves an overall 4% expansion and an iris type of movement of viral protein VP1 to open up a 10-Å-diameter channel on the fivefold axis to allow exit of the RNA genome. The β-cylinders formed by the N termini of the VP3 molecules inside the capsid on the fivefold axis all open up in HRV2, but we propose that only one opens up in HRV14. The release of VP4 is less efficient in HRV14 than in HRV2, and the N termini of VP1 may exit at different points. The N-terminal loop of VP2 is modified in both viruses, probably to detach the RNA, but it bends only inwards in HRV2.

A key event in the life cycle of any virus is the delivery of its genome into the appropriate compartment of the host cell for reproduction. This involves the recognition of the cell via a specific cell surface receptor(s) and the passage of the genome across at least one membrane barrier. The receptor molecules used by a number of different viruses have been identified, and for certain viruses, the medium resolution structure of the virus-receptor complex has been determined (9, 10, 16, 17, 20, 23, 26). The rhinoviruses are particularly interesting in that they fall into two different groups according to their cellular receptors; certain rhinoviruses (the major group of human rhinoviruses [HRVs]) use intercellular adhesion molecule 1 (ICAM-1) (33), and others (the minor group of HRVs) use members of the low-density lipoprotein (LDL) receptor family (21). These receptor molecules bind to different sites on the viral surface and play different roles in virus uncoating (20, 23, 31). ICAM-1 binds in a depression or canyon around each fivefold axis, while the LDL receptors bind on a star-shaped dome on each of the fivefold axes. ICAM-1 catalyzes the release of the single-stranded RNA genome for some major-group HRVs (13), while the LDL receptor does not (7, 21). Uncoating of the minor-group HRVs is triggered by the low pH of the late endosome (27).

The rhinoviruses are members of the *Picornaviridae* family and have a positive-sense RNA genome. They are the major cause of the common cold. The capsid is composed of 60 copies each of four viral proteins (VPs), VP1, VP2, VP3, and VP4, on a T=1 (or pseudo T=3) lattice (29). The N-terminal extensions of the VPs 1, 2, and 3 are each located in the interior of the capsid. The C termini are located on the exterior surface of the capsid. VP4, a small (8-kDa) protein which is only partially ordered, lies entirely within the capsid (2). The N termini interact with one another and with the cores of the other capsid proteins to give added stability to the capsid. Previous work on HRV2 revealed that each of these N termini undergoes a conformational change which plays a role in the uncoating of the virus. It is known from biochemical (36) and mass spectroscopy (6, 25) experiments that during uncoating VP4 is released and the N terminus of VP1 is externalized.

The assembly and uncoating of polioviruses during infection have been more extensively studied than those of any other picornavirus. The structure of the empty poliovirus capsid assembly intermediate prior to maturation cleavage of VP0 into VP2 and VP4 is the only atomic structure of an empty picornavirus capsid resolved to date (4). The overall size, the outer surface, and most of the protein shell of the empty poliovirus capsid are practically identical to those of the mature capsid. However, the N-terminal extension of VP1 and the segment of VP0 that becomes VP4 and the N-terminal extension of VP2, which are disordered in the empty capsid, become ordered in the mature capsid and interact with neighboring VPs, thus increasing virion stability. Also, part of VP4 moves by roughly 20 Å after cleavage. The structure of the empty poliovirus capsid after uncoating, determined to 22-Å resolution by cryoelectron microscopy (cryo-EM) (5), reveals that after release of the RNA the empty capsid expands by 4%. While each of the capsid proteins apparently moves relative to one another, no opening on the fivefold axis is observed. The authors proposed that openings on both the pseudo threefold axis at the

* Corresponding author. Mailing address: Institut de Biologie Structurale Jean-Pierre Ebel, 41 rue Jules Horowitz, 38027 Grenoble, France. Phone: (33) (0) 4 38784568. Fax: (33) (0) 4 38785494. E-mail: elizabeth.hewat@ibs.fr.

intersection of VP1, VP2, and VP3 and the fivefold axis are involved in the exit of VP4, the N terminus of VP1, and the RNA. This is largely similar to previously proposed models (12, 14, 24) in which the RNA is hypothesized to exit via the fivefold axis and VP4 and the N terminus of VP1 are hypothesized to exit via the pseudo threefold axis and/or the fivefold axis.

With the use of cryo-EM and X-ray data, it has been shown (18) that HRV2, a minor-group HRV, undergoes concerted structural changes during uncoating. The transformation from full to empty capsid involves an overall 4% expansion of the radius with an additional outward movement on the fivefold axes. The two proteins around the fivefold axis, VP1 and the N terminus of VP3, make an iris type of movement to open up a 10-Å-diameter channel to allow exit of the RNA genome. The N terminus of VP1 apparently exits the capsid at the pseudo threefold axis, and a remarkable modification occurs at the twofold axes where the N-terminal loop of VP2 bends inwards. It was proposed that this large movement of the N-terminal VP2 loop is involved in the release of the RNA stacked against Trp 2038 (residue 38 of VP2) and possibly in the expulsion of the RNA. The conserved nature of the Trp 2038, in three different genera of *Picornaviridae*, and the observation that RNA is visibly stacked against it in eight different capsid structures, including that of HRV14, led to the prediction of similar roles for the N-terminal VP2 loop in all these viruses. In a more recent study using the same techniques for the major-group HRV3 in complex with ICAM-1, Xing and colleagues (34) also found a 4% increase in the diameter of the empty capsid while the ICAM-1 remains bound. At 23-Å resolution, they modeled an opening on the pseudo threefold axis but did not see any opening on the fivefold axis. They proposed that the bound receptor maintains the capsid in an expanded state to allow genome release.

In view of the known differences in the interactions of major- and minor-group HRVs with their receptors and the proposed similarity of the uncoating processes of these viruses, it is of interest to make a more detailed comparison of the uncoating processes of major- and minor-group HRVs. We have studied the uncoating of the major-group HRV14 by determining the structure of the empty HRV14 capsid by using cryo-EM and three-dimensional reconstruction. The combination of the cryo-EM-derived map and the atomic structure of the native HRV14 determined by X-ray crystallography (15) allowed us to model some of the conformational changes in the empty HRV14 capsid. A comparison of HRV14 and HRV2 empty capsids shows both similarities and unexpected differences.

MATERIALS AND METHODS

Preparation of frozen hydrated specimens of empty HRV14. HRV14 was grown in Rhino-HeLa cells in suspension culture and purified as described previously for HRV2 (20). To prepare empty HRV14 particles, a suspension of HRV14 (~1 mg/ml) in 50 mM Tris-HCl, pH 7.4, was heated to 55°C for 30 min immediately prior to preparation of the cryo-EM specimens.

Preparation of frozen hydrated specimens. Frozen hydrated specimens were prepared on holey carbon grids as previously described (19). Specimens were photographed at a temperature of close to −175°C by using an Oxford cryoholder CT3500 in a JEOL 2010F field emission gun operating at 200 kV. Defocus image pairs were obtained under low-dose conditions (<10 e/Å^2) at a nominal magnification of 40,000 times at underfocus values ranging from 1.1 to 2.4 μm.

Image analysis. Selected images were digitized on a Zeiss scanner with a pixel size of 7 μm on the micrograph. The pixel size was internally calibrated with the 11.5-Å-layer line of tobacco mosaic virus to be 1.77 Å. The virus particles were selected and sorted visually into two different categories, one class of empty capsids (density of the outer capsid ring was greater than the density inside) and another class of nearly empty capsids (density of the outer capsid ring and density inside were roughly the same). The map of empty HRV2 particles obtained in a previous study (20) was used as a starting model for the analysis of empty HRV14 particles. All subsequent refinement of particle origin and orientation was performed using the model-based polar Fourier transform programs (3). The program CTFMIX (11) was used to correct for contrast transfer function effects, to combine defocus pairs for orientation and origin refinement, and to complete the final Fourier-Bessel reconstruction. In the final reconstruction of empty HRV14, 2,173 image defocus pairs from four micrographs were retained out of a total of 4,164 pairs in the combined set. Of the empty set, 1,048 particles were retained, and 1,125 particles of the nearly empty set were retained. The resolution, estimated by Fourier shell correlation of reconstructions from half data sets, was 12.5 Å with the criterion of 0.5 and 9.5 Å with a 0.1 criterion for the combined set.

Fitting HRV14 X-ray structures of VP1, VP2, and VP3 to the cryo-EM–reconstructed density. The atomic structure of each VP was first fitted visually to the contrast transfer function-corrected cryo-EM map by using the program "O" (22). VP1 minus the 62 N-terminal residues (VP1-Δ) was used rather than the entire VP1 molecule since no density for these residues is present in the map. VP1-Δ, VP2, and VP3 were then fitted in turn with the program EMfit (28) by using difference maps. In order to fit VP1-Δ, for example, the existing best-fit positions of VP2 and VP3 were used to calculate the 12-Å-resolution map of the entire virus (without VP1-Δ) by using the icosahedral symmetry operators and the CCP4 program suite. The difference map for the cryo-EM map of the empty capsid and the simulated capsid map of VP2 and VP3 was produced after normalizing the standard deviations. Thus, a difference map of the density of VP1-Δ only was created to fit VP1-Δ. A best fit for VP1-Δ was obtained by maximizing the average density per atomic site for VP1-Δ, minimizing the number of atoms located in below-average density, and minimizing clashes of VP1 with the neighboring VP1 molecules by using EMfit. By using the difference map with the densities of VP2 and VP3 removed, clashes with VP2 and VP3 were to some extent also minimized. Only carbon alpha atoms were considered. This process was repeated to convergence. In fact, on the third cycle the positions were stable (unchanged). Figures were produced using Amira (see Fig. 1 and 2; Indeed-Visual Concepts GmbH, Berlin, Germany) and the program "O" (see Fig. 2 and 3).

RESULTS

Cryo-EM images of HRV14. In cryo-EM images, the empty HRV14 particles appear as hollow spheres while the native virions appear as solid spheres. Some of the empty HRV14 particles appear to be quite empty while others have a slightly denser interior. The particles can easily be sorted visually into these two categories (see Materials and Methods). The empty HRV14 capsids showed less tendency to further disintegrate compared with the empty HRV2 when prepared under the same conditions (i.e., incubation for 30 min at 55°C). Increasing the incubation time to 45 min and the temperature to 60°C did not significantly increase the number of empty particles.

Comparison of the native and empty HRV14 capsids. Internal calibration of the magnification of the EM images revealed that the empty capsid had expanded by 4%. We compared the native HRV14 capsid, simulated from X-ray data with a resolution cutoff at 12 Å and a temperature factor of 500 Å^2, and the reconstructed empty HRV14 capsid. Since the RNA structure was not determined by X-ray crystallography, it was not included in the simulated map of the native HRV14 capsid, which therefore appears completely empty. The native and empty capsids had the same general features: a star-shaped dome on the fivefold axes surrounded by a depression or canyon with a triangular plateau centered on each of the threefold axes (Fig. 1A and C). On the exterior surface, the major change was that the dome on the fivefold axes had become enlarged and swiveled around in a manner very reminiscent of

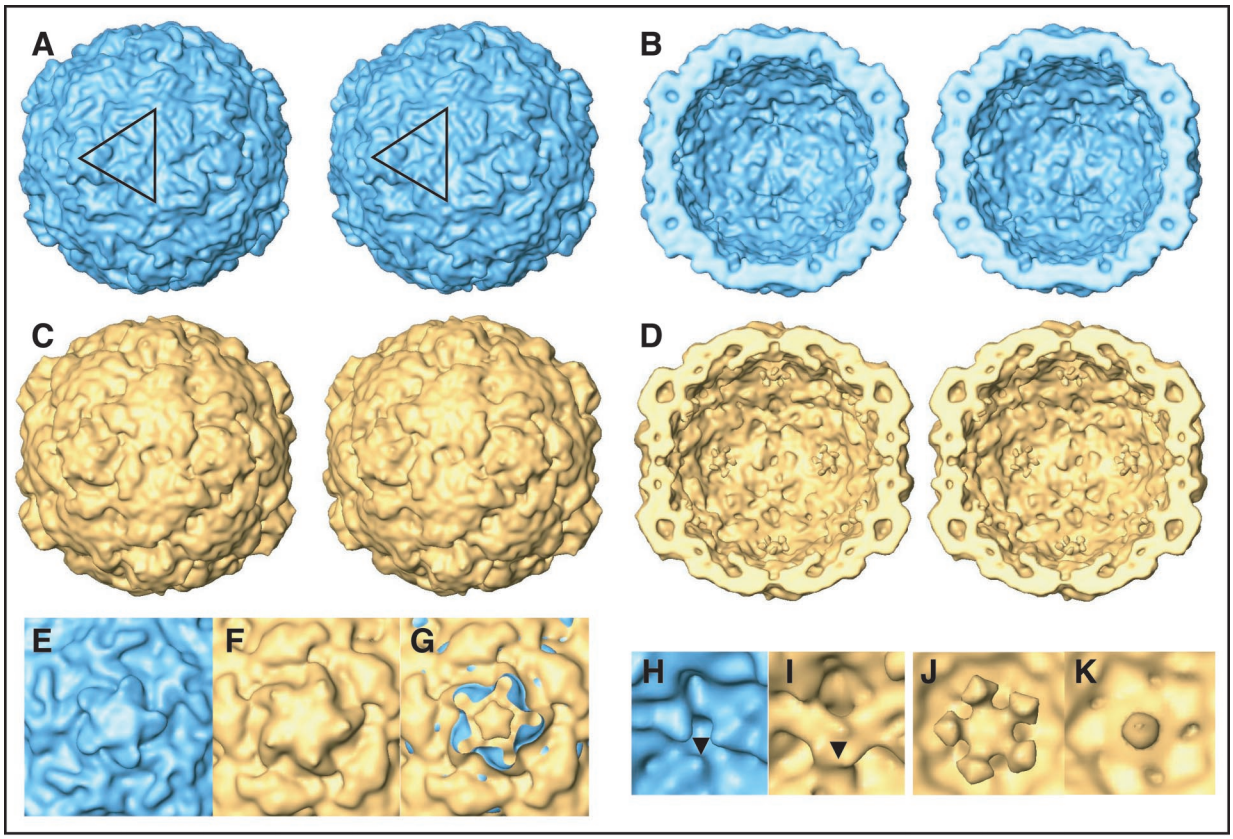

FIG. 1. Surface representations of the X-ray map of native HRV14 (blue) and of the reconstructed cryo-EM map of the nearly empty HRV14 (gold). One icosahedral asymmetric unit is indicated by triangles in panel A. The map of the native HRV14 capsid is limited to 12-Å resolution with a temperature factor of 500 Å^2 and was calculated without the RNA, VP4, and the 62 N-terminal residues of VP1. (A and C) Whole virus. (B and D) Interior of the capsid with the front half cut away. (E and F) Close-up views down a fivefold axis. (G) Comparison between the native and nearly empty capsids with a section removed near the apex of the fivefold axis of native HRV14. A clockwise rotation of the dome of the empty capsid is apparent. (H and I) Close-up views of the threefold axes (indicated by arrowheads) from inside the capsid (side view with the same orientation as that in panels A and C). The interiors of the nearly empty (J) and empty (K) capsid reconstructions at the fivefold axes show marked differences.

the HRV2 empty capsid (Fig. 1E, F, and G). In the interior of the capsid, differences were evident on each of the symmetry axes (Fig. 1B, D, H, and I). Interestingly, the comparison of the interiors of the empty capsids of HRV2 and HRV14 also revealed considerable differences on each of the axes.

It is instructive to compare the native HRV14 capsid, simulated from X-ray data, and the reconstructed empty HRV14 capsid reduced in size by 4% so that it has practically the same size as the native capsid (Fig. 2). Differences on the inside of the capsid were quite remarkable. There was density lining the inside of the native capsid that was missing from the empty capsid (Fig. 2A, B, C, and D). This missing density corresponds to the ~62 N-terminal residues of VP1 and the 39 residues of VP4 identified in the X-ray structure and demonstrates that these chains were absent, or at least disordered. A simulation of the native capsid without the 62 N-terminal residues of VP1 and the 39 residues of VP4 agreed much better with the interior of the empty capsid (Fig. 2A and B). The bubble of low (solvent) density, which we attribute to the pocket in VP1, was also rotated clockwise and was reduced in size (Fig. 2F). The bubble of low density located on the pseudo threefold axis, i.e., at the intersection of VP1, VP2, and VP3, was essentially unchanged (Fig. 2F). This differs from the empty HRV2 capsid, where the filling of this bubble was interpreted to result from the exiting of the N terminus of VP1 at this location.

On the fivefold axis, the density from the β-cylinder formed by the N termini of VP3 was apparently still in place and an additional density below the β-cylinder was also apparent. This density was comparable to the average density in the capsid. It had diminished in the empty capsid compared with that in the nearly empty capsids and was the only really significant change between these categories of capsids (Fig. 1J and K). We attribute this extra density to the 28 N-terminal residues of each VP4 molecule not resolved in the X-ray structure due to the residues' lack of order. It is remarkable that the 39 residues of VP4 resolved by X-ray crystallography were seen to be "attached" to the density on the fivefold axis (Fig. 2E and F).

Additional density on the threefold axes at the inner surface of the empty capsid extended from the N termini of the three surrounding VP2 molecules and linked these molecules together (Fig. 1H and I and 2G). We attribute this finding to the seven N-terminal residues of VP2 not resolved in the X-ray structure. On the twofold axes, a redistribution of the density had occurred, opening up a gap on the inside surface of the capsid (Fig. 2A, B, and F and 3B). However, there was no large

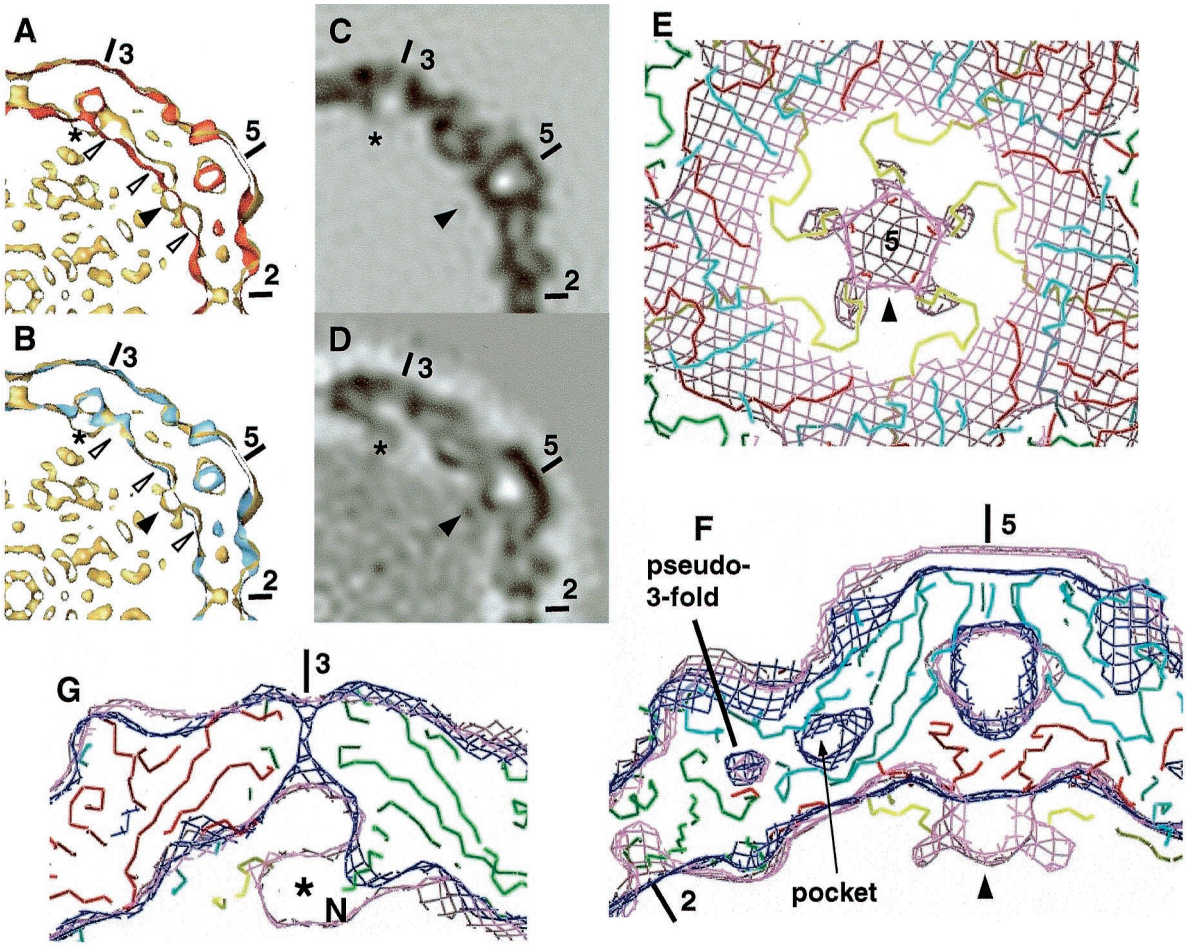

FIG. 2. Sections of the X-ray map of native HRV14 and of the reconstructed cryo-EM map of the nearly empty HRV14 reduced in size by 4% for comparison. The two-, three-, and five-fold axes are indicated as appropriate. Asterisks and closed arrowheads indicate the positions of additional density inside the empty capsid on the three- and fivefold axes, respectively. (A and B) Fifteen-Å-thick sections of the scaled HRV14 empty capsid (gold) and the native HRV14 capsid simulated with (red) and without (blue) VP4 and the N terminus of VP1. Open arrowheads indicate the positions of VP4 and the N terminus of VP1. In the absence of these chains, the two structures match much better on the inner surface (B). (C and D) Central sections of the X-ray map of native HRV14 minus VP4 and the N terminus of VP1 (C) and of the reconstructed cryo-EM map of the size-matched empty HRV14 (D). (E, F, and G) Sections of the size-matched HRV14 nearly empty capsid (pink) and the native HRV14 capsid simulated without VP4 and the N terminus of VP1 (dark blue). C_α backbones of the known X-ray structures of VP1, VP2, VP3, and VP4 are depicted in blue, green, red, and yellow, respectively, in their positions in the native capsid. In panels E and F, the VP4 molecules are seen to be attached to the additional density on the fivefold axis. Panel F demonstrates missing density inside the empty capsid on the twofold axis compared with the density in the native capsid. The bubble of low density on the pseudo threefold axis is unchanged, and the pocket in VP1 is visible in the native capsid but is not visible in the empty capsid in this section as it is displaced and smaller. (G) The N terminus of VP2 is seen to point into the additional density on the threefold axis, which is sufficient to accommodate the seven disordered N-terminal residues of VP2.

movement of density inwards at the twofold axes, unlike that observed in the case of HRV2.

Modeling the empty HRV14 capsid. After removal of the 62 residues of the N terminus of VP1 to give VP1-Δ, each of the capsid proteins VP1-Δ, VP2, and VP3 were fitted first visually to the correctly scaled cryo-EM map of the nearly empty particles. This first fit was then refined using EMfit (28) (Table 1).

VP1. VP1-Δ had moved more than any of the other proteins. It had been cantilevered up and rotated around the fivefold axis to open a 10-Å channel. The bubble of low density, which we identify as the pocket, was much smaller than in the native capsid and was not well positioned in VP1. The poor fit about the pocket suggests that the pocket collapsed and VP1 made a hinge-type movement (Fig. 3A) as proposed previously (23). The C terminus of VP1 lay over VP3 on the outside surface of the capsid and was also not well positioned as it clashed with VP3. This is not surprising for a single strand which easily moves around. Unlike the case of the empty HRV2 capsid, there was no evidence that this N terminus of VP1 exits the

TABLE 1. Results of fitting atomic structures of VPs to the cryo-EM map of empty HRV14 using EMfit[a] (28)

Protein	Sumf	Clash	Den
VP1-Δ	59.2	0.0	1.8
VP2	62.6	0.0	2.2
VP3	59.5	0.0	2.6

[a] Sumf is the average density at the atomic positions as a percentage of the maximum density. Clash is the percentage of atoms per VP that have a steric clash with other examples of the same VP. Den is the percentage of atoms per VP in negative density.

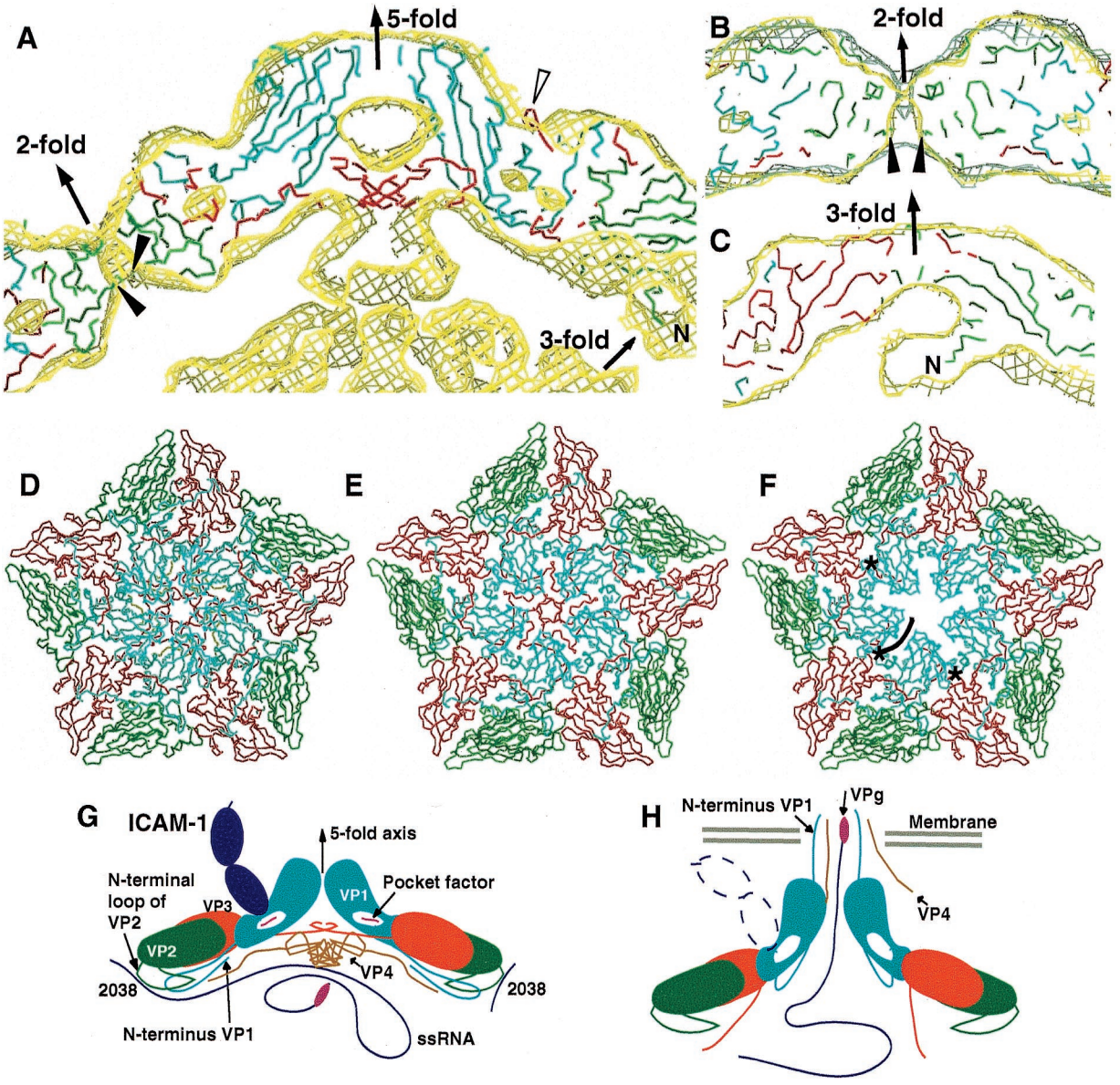

FIG. 3. Fit of VPs in the empty capsid of HRV14 at the correct size (gold) showing the C_α backbones of VP1-Δ (blue), VP2 (green), and VP3 (red). (A) Overall view with the two-, three-, and fivefold axes marked. The C terminus of VP3 that lies outside the density of the empty capsid is indicated with an open arrowhead. (B and C) Views of the two- and threefold axes. The N-terminal loop of VP2 encroaches on the region of low density at the twofold axis (indicated by arrowheads in panels A and B), so the N-terminal loop of VP2 has most probably been modified. In panel B, the grey lines represent the map simulated from the best-fit positions. The position of the N terminus of VP2 is marked by an N in panels A and C. The VPs on one icosahedral pentamer are shown in panel D for the native capsid and in panels E and F for the best-fit empty capsid. In panel F, the 20 N-terminal residues of VP3 have been removed to show that this would allow exit of the N terminus of VP1 as indicated in black. In three VP1 molecules, the 62nd residue is marked with an asterisk. (G and H) Schematic diagrams of the reorganization of the HRV14 capsid during release of the RNA. In the native capsid (G), the RNA is bound to Trp 2038 of VP2 and the pocket is filled with a pocket factor. The cellular receptor ICAM-1 binds in the canyon in a two-step process which expels the pocket factor and induces a hinge-type movement of VP1 (23) as the capsid undergoes a 4% expansion (H). Each VP1 protein is cantilevered up and away from the fivefold axis while it swivels around to open a 10-Å-diameter channel. The β-cylinders formed by the N termini of VP3 on each fivefold axis mostly remain in place. We postulate that at least one such β-cylinder must be modified to allow exit of the VP4 molecules, the N termini of VP1, and the RNA. We propose that the N termini of the VP1 molecules exit the capsid along channels which open up between neighboring VP1 molecules and become anchored in the membrane to retain the HRV14 close to the membrane. In association with VP4, which probably exits via the fivefold axis, they destroy the endosomal membrane and thereby releases the RNA into the cytosol (31). The N-terminal loop of VP2 is modified to detach the RNA bound to the conserved Trp 2038.

capsid at the pseudo threefold axis at the junction of VP1, VP2, and VP3, since the bubble of low density on the pseudo threefold axis was essentially unchanged (Fig. 2F). We have located another possible exit site (Fig. 3F). There was a channel of unfilled density between the neighboring VP1 molecules. This channel was blocked by the N terminus of VP3 which we suppose must be displaced to allow passage of the VP1 N terminus (Fig. 3D, E, and F). The additional density on the

fivefold axis on the outer viral surface is difficult to interpret (Fig. 2D and F). It may be due to strands of VP4 attached to the surface of the channel formed by VP1. This agrees with our observation that 80S particles obtained upon incubation of the virus at 55°C followed by ultracentrifugation were not completely devoid of VP4.

VP2. The case of VP2 is particularly interesting. Inside the capsid on the threefold axis, there was density not present on the X-ray-derived map. However, the seven N-terminal residues of VP2 were not resolved in the X-ray structure presumably because they were not sufficiently well ordered. The three N-terminal strands of VP2, up to residue 2008, pointed towards this extra density, and three 7-amino-acid strands were the correct size to account for it (Fig. 2G and 3C). Thus, we attribute this additional density on the threefold axes to these amino acid residues missing in the X-ray structure. In the empty capsid, both VP2 and VP3 had not moved away from the threefold axis by more than about 1 Å, though VP2 and VP3 had moved outwards radially by roughly 6 Å. While there is not sufficient information to model these three strands of the N termini of VP2, our results suggest that they remain linked together, thus helping to maintain the integrity of the capsid while it expands. This is reminiscent of several plant viruses, which have VP extensions linked on the icosahedral axes that serve the same purpose (32). A reinspection of the cryo-EM map of native and empty HRV2 revealed a similar phenomenon with the difference that, since11 residues were missing, the strands were less well ordered and so of lower density.

The rigid body fit of VP2 was not good on the twofold axis (Fig. 3B). There was a gap which had opened up on the inside of the capsid which was not accounted for with a rigid body fit. The N-terminal loop of VP2 (amino acids 2036 to 2063) encroached on the gap, and there was a small region of unoccupied density at the tip of the N-terminal loop of VP2. Unlike that in the empty HRV2 capsid, there was no evidence of a large-scale movement of the N-terminal loop of VP2. Therefore, these results imply that the N-terminal loop of VP2 had undergone a plastic deformation. Since the N-terminal loops of VP2, which face each other across the twofold axis, are anchored at two different threefold axes, they must be subjected to some strain as the capsid expands.

VP3. The fit of the core of VP3 was in general very good (Fig. 2G). The six residues of the C termini of VP3, which normally lie above VP1 on the outer surface of the virus, were found outside the density (Fig. 3A). They were apparently disordered. The 40-residue-long N terminus of VP3 wended its way on the inner surface of the capsid to the fivefold axis, where it formed a β-cylinder with four other VP3 N termini (Fig. 3A). This cylinder was apparently unchanged and still in place. The fit of this long chain was imperfect, which was to be expected since it must be modified during expansion of the capsid to adapt to the increased size and other changes of the capsid.

DISCUSSION

Processes of uncoating of HRV2 and HRV14 showed many similarities. Both involved a cooperative movement of all the capsid proteins, leading to a 4% expansion of the capsid as seen for other picornaviruses (5, 34). The five copies of VP1 surrounding each fivefold axis were cantilevered up and swiveled around to open up a 10-Å channel on each axis. The 60 or so N-terminal residues of VP1 and the ordered C-terminal part of VP4 were not visible in the cryo-EM density map. However, in all other modifications of the VPs, there were differences between these major- and minor-group viruses. For HRV2, a density increase at the pseudo threefold axis upon expansion suggested that this axis was the point of exit of the N terminus of VP1. In contrast, the low density at the pseudo threefold axis of HRV14 remained unchanged, indicating that this was not the exit pathway for HRV14. Since the pseudo threefold axis lies within the footprint of the ICAM-1 receptor molecule, the N terminus of VP1 will not be able to exit at this point if a receptor molecule is bound. Another possible exit path has been identified between two neighboring copies of VP1 on the north rim of the canyon (Fig. 3F). There was strong evidence that the N-terminal loop of VP2 in HRV14 had changed its conformation but it had not also made a large inwards movement as in HRV2. This conformational change may be involved in the release of the RNA from Trp 2038, though probably not in the expulsion of the RNA. Most striking was the difference on the fivefold axis where the VP3 β-cylinder was enlarged in HRV2 but was still present and apparently unchanged in HRV14. While there was no sign of clearly localized density corresponding to VP4 in HRV2, there was very strong density inside the empty HRV14 on the fivefold axis that we attributed to the N-terminal half of VP4, which was disordered in the X-ray structure. This is in accord with the structural results for HRV16, where the N-terminal part of VP4 was better ordered and was seen to be located at the fivefold axis. In cryo-EM reconstructions of native HRVs, there is also a density at this location (18).

The cooperative movement of the VP1 molecules around the fivefold axis to open up a channel make it the most probable exit site for the RNA. However, the rearrangement of VP2 at the twofold axis also presents a possible point of exit. The location of the VP4 on the fivefold axis and the anchorage point of the N terminus of VP1 near the fivefold axis favor an exit site closer to the fivefold axis than the twofold axis.

It is clear from the cryo-EM map that the N terminus of VP1 and the C-terminal half of VP4 were detached from the interior of the capsid but that many of the VP4 molecules remained attached at the fivefold axes. The detached part of VP4 must be spatially and/or temporally disordered and so will account for a proportion of the material seen in the not-quite-empty capsids. Some of the detached N termini of VP1 may also remain inside the capsid. The externalization of VP4 is apparently progressive. It is probable that VP4 can exit the capsid only via the fivefold axis when the VP3 β-cylinder is displaced. This observation is in accord with results of Casasnovas and Springer (8), who found that the empty HRV3 capsids, i.e., the 80S particles, are heterogeneous and retain from 68 to 26% of their VP4.

In the empty capsid, VP1 opened to form a channel capable of allowing the passage of the RNA, but the VP3 β-cylinder apparently remained largely unchanged even when most if not all of the RNA had been ejected. So how does the RNA exit the capsid? We note that the cryo-EM map is averaged over all icosahedral symmetry-related positions, so a difference at just one position will not be easily detected. Thus, it is possible that just one β-cylinder moves to allow passage of the associated

VP4 and the RNA. Such a movement may be temporary or permanent. Thus, while in general all the VPs make a concerted cooperative movement in uncoating, we suggest that the VP3 N terminus is an exception to this rule. Somehow an asymmetry may be introduced, possibly by the position of the VPg on the 5′ end of the RNA or the location of bound receptor molecules. In a cryo-EM study of the uncoating of poliovirus, density was also observed on the fivefold axis of the 80S particle and interpreted as the VP3 β-cylinder (5). Regarding the behavior of the VP3 β-cylinder, poliovirus and HRV14 appear to be similar, while HRV2 shows a different comportment. However, regarding movement of the N-terminal loop of VP2, poliovirus resembles HRV2 rather than HRV14 (5, 18). We note that in both of the cryo-EM studies of poliovirus (5) and HRV3 (35), no channel on the fivefold axis was detected. However, as both of these studies were limited to roughly 22-Å resolution, it is possible that higher resolution may reveal a channel. Xing and colleagues proposed that the bound receptor maintains the capsid in an expanded state to allow genome release (35). However, this does not appear to be the case for HRV14 empty capsids since they are in an expanded state even in the absence of ICAM-1. HRV14 and HRV3 belong to genus B, whereas most of the other HRVs, including HRV2, are genus A; this classification is based on phylogeny but correlates well with sensitivity towards distinct classes of antiviral agents, which is reflected in the geometry of the hydrophobic pocket accommodating the drugs (1, 30). Therefore, not all members of the major or minor groups of HRVs will necessarily have the same characteristics.

Our results indicate that the uncoating of HRV14 follows similar lines as that of HRV2 even though it is triggered by different means and follows different kinetics. As proposed by Kolatkar and colleagues (23), we suppose that ICAM-1 binds to the major-group HRVs in a two-step process involving expulsion of the natural pocket factor and a hinge-type movement of VP1 about the pocket away from the fivefold axis, thus opening a channel for the RNA to exit. This proposed role of the pocket factor in uncoating, and even its presence in native HRV14, does, however, require verification. The N terminus of VP1 exits most probably between neighboring VP1 molecules on the star-shaped dome to be inserted into the cellular membrane. Only one or two of the VP3 β-cylinders on the fivefold axes are modified to allow passage of the underlying VP4, the VP1 N terminus, and the RNA. The hydrophobic VP4 and the N termini of VP1 must then be inserted into the cellular membrane to facilitate the passage of the RNA across the membrane or to disrupt the membrane altogether (31).

ACKNOWLEDGMENTS

We thank M. G. Rossmann for supplying the source code for his program EMfit and for all his generous, ever-ready help in getting the program up and running. The help of M. G. Rossmann's students Chuan (River) Xiao and Suchetana (Tulli) Mukhopadhyay was also much appreciated. We thank F. Metoz for assistance in running the computers, J. F. Conway for the CTFMIX programs, T. S. Baker for supplying the polar Fourier transform programs employed, and I. Goesler for preparing HRV14.

The fitting was performed on a personal computer bought with the Atipe funds awarded to James Conway. The work was supported by the Austrian Science Foundation grant no. P14053-MOB to D.B.

REFERENCES

1. **Andries, K., B. Dewindt, J. Snoeks, R. Willebrords, R. Stokbroekx, and P. J. Lewi.** 1991. A comparative test of fifteen compounds against all known human rhinovirus serotypes as a basis for a more rational screening program. Antivir. Res. **16:**213–225.
2. **Arnold, E., and M. G. Rossmann.** 1990. Analysis of the structure of a common cold virus, human rhinovirus 14, refined at a resolution of 3.0 A. J. Mol. Biol. **211:**763–801.
3. **Baker, T. S., and R. H. Cheng.** 1996. A model-based approach for determining orientations of biological macromolecules imaged by cryoelectron microscopy. J. Struct. Biol. **116:**120–130.
4. **Basavappa, R., R. Syed, O. Flore, J. P. Icenogle, D. J. Filman, and J. M. Hogle.** 1994. Role and mechanism of the maturation cleavage of VPO in poliovirus assembly: structure of the empty capsid assembly intermediate at 2.9 angstrom resolution. Protein Sci. **3:**1651–1669.
5. **Belnap, D. M., D. J. Filman, B. L. Trus, N. Cheng, F. P. Booy, J. F. Conway, S. Curry, C. N. Hiremath, S. K. Tsang, A. C. Steven, and J. M. Hogle.** 2000. Molecular tectonic model of virus structural transitions: the putative cell entry states of poliovirus. J. Virol. **74:**1342–1354.
6. **Bothner, B., X. F. Dong, L. Bibbs, J. E. Johnson, and G. Siuzdak.** 1998. Evidence of viral capsid dynamics using limited proteolysis and mass spectrometry. J. Biol. Chem. **273:**673–676.
7. **Brabec, M., G. Baravalle, D. Blaas, and R. Fuchs.** 2003. Conformational changes, plasma membrane penetration, and infection by human rhinovirus type 2: role of receptors and low pH. J. Virol. **77:**5370–5377.
8. **Casasnovas, J. M., and T. A. Springer.** 1994. Pathway of rhinovirus disruption by soluble intercellular adhesion molecule 1 (ICAM-1): an intermediate in which ICAM-1 is bound and RNA is released. J. Virol. **68:**5882–5889.
9. **Chipman, P. R., M. Agbandje-McKenna, S. Kajigaya, K. E. Brown, N. S. Young, T. S. Baker, and M. G. Rossmann.** 1996. Cryo-electron microscopy studies of empty capsids of human parvovirus B19 complexed with its cellular receptor. Proc. Natl. Acad. Sci. USA **93:**7502–7506.
10. **Chiu, C. Y., P. Mathias, G. R. Nemerow, and P. L. Stewart.** 1999. Structure of adenovirus complexed with its internalization receptor, $\alpha_v\beta5$ integrin. J. Virol. **73:**6759–6768.
11. **Conway, J. F., and A. C. Steven.** 1999. Methods for reconstructing density maps of "single" particles from cryoelectron micrographs to subnanometer resolution. J. Struct. Biol. **128:**106–118.
12. **Filman, D. J., R. Syed, M. Chow, A. J. Macadam, P. D. Minor, and J. M. Hogle.** 1989. Structural factors that control conformational transitions and serotype specificity in type 3 poliovirus. EMBO J. **8:**1567–1579.
13. **Greve, J. M., C. P. Forte, C. W. Marlor, A. M. Meyer, H. Hooverlitty, D. Wunderlich, and A. McClelland.** 1991. Mechanisms of receptor-mediated rhinovirus neutralization defined by two soluble forms of ICAM-1. J. Virol. **65:**6015–6023.
14. **Hadfield, A. T., W. M. Lee, R. Zhao, M. A. Oliveira, I. Minor, R. R. Rueckert, and M. G. Rossmann.** 1997. The refined structure of human rhinovirus 16 at 2.15 angstrom resolution: implications for the viral life cycle. Structure **5:**427–441.
15. **Hadfield, A. T., M. A. Oliveira, K. H. Kim, I. Minor, M. J. Kremer, B. A. Heinz, D. Shepard, D. C. Pevear, R. R. Rueckert, and M. G. Rossmann.** 1995. Structural studies on human rhinovirus 14 drug-resistant compensation mutants. J. Mol. Biol. **253:**61–73.
16. **He, Y., V. D. Bowman, S. Mueller, C. M. Bator, J. Bella, X. Peng, T. S. Baker, E. Wimmer, R. J. Kuhn, and M. G. Rossmann.** 2000. Interaction of the poliovirus receptor with poliovirus. Proc. Natl. Acad. Sci. USA **97:**79–84.
17. **He, Y., P. R. Chipman, J. Howitt, C. M. Bator, M. A. Whitt, T. S. Baker, R. J. Kuhn, C. W. Anderson, P. Freimuth, and M. G. Rossmann.** 2001. Interaction of coxsackievirus B3 with the full length coxsackievirus-adenovirus receptor. Nat. Struct. Biol. **8:**874–878.
18. **Hewat, E., E. Neumann, and D. Blaas.** 2002. The concerted conformational changes during human rhinovirus 2 uncoating. Mol. Cell **10:**317–326.
19. **Hewat, E. A., and D. Blaas.** 1996. Structure of a neutralizing antibody bound bivalently to human rhinovirus 2. EMBO J. **15:**1515–1523.
20. **Hewat, E. A., E. Neumann, J. F. Conway, R. Moser, B. Ronacher, T. C. Marlovits, and D. Blaas.** 2000. The cellular receptor to human rhinovirus 2 binds around the 5-fold axis and not in the canyon: a structural view. EMBO J. **19:**6317–6325.
21. **Hofer, F., M. Gruenberger, H. Kowalski, H. Machat, M. Huettinger, E. Kuechler, and D. Blaas.** 1994. Members of the low density lipoprotein receptor family mediate cell entry of a minor-group common cold virus. Proc. Natl. Acad. Sci. USA **91:**1839–1842.
22. **Jones, T. A., J. Y. Zou, S. W. Cowan, and M. Kjeldgaard.** 1991. Improved methods for building protein models in electron density maps and the location of errors in these models. Acta Crystallogr. A **47:**110–119.
23. **Kolatkar, P. R., J. Bella, N. H. Olson, C. M. Bator, T. S. Baker, and M. G. Rossmann.** 1999. Structural studies of two rhinovirus serotypes complexed with fragments of their cellular receptor. EMBO J. **18:**6249–6259.
24. **Lentz, K. N., A. D. Smith, S. C. Geisler, S. Cox, P. Buontempo, A. Skelton,**

J. Demartino, E. Rozhon, J. Schwartz, V. Girijavallabhan, J. O'Connell, and E. Arnold. 1997. Structure of poliovirus type 2 Lansing complexed with antiviral agent Sch48973: comparison of the structural and biological properties of the three poliovirus serotypes. Structure **5:**961–978.

25. **Lewis, J. K., B. Bothner, T. J. Smith, and G. Siuzdak.** 1998. Antiviral agent blocks breathing of the common cold virus. Proc. Natl. Acad. Sci. USA **95:**6774–6778.
26. **Olson, N. H., P. R. Kolatkar, M. A. Oliveira, R. H. Cheng, J. M. Greve, A. McClelland, T. S. Baker, and M. G. Rossmann.** 1993. Structure of a human rhinovirus complexed with its receptor molecule. Proc. Natl. Acad. Sci. USA **90:**507–511.
27. **Prchla, E., E. Kuechler, D. Blaas, and R. Fuchs.** 1994. Uncoating of human rhinovirus serotype 2 from late endosomes. J. Virol. **68:**3713–3723.
28. **Rossmann, M. G.** 2000. Fitting atomic models into electron-microscopy maps. Acta Crystallogr. D **56:**1341–1349.
29. **Rossmann, M. G., E. Arnold, J. W. Erickson, E. A. Frankenberger, J. P. Griffith, H. J. Hecht, J. E. Johnson, G. Kamer, M. Luo, A. G. Mosser, R. R. Rueckert, B. Sherry, and G. Vriend.** 1985. Structure of a human common cold virus and functional relationship to other picornaviruses. Nature **317:** 145–153.
30. **Savolainen, C., S. Blomqvist, M. N. Mulders, and T. Hovi.** 2002. Genetic clustering of all 102 human rhinovirus prototype strains: serotype 87 is close to human enterovirus 70. J. Gen. Virol. **83:**333–340.
31. **Schober, D., P. Kronenberger, E. Prchla, D. Blaas, and R. Fuchs.** 1998. Major and minor receptor group human rhinoviruses penetrate from endosomes by different mechanisms. J. Virol. **72:**1354–1364.
32. **Speir, J. A., S. Munshi, G. Wang, T. S. Baker, and J. E. Johnson.** 1995. Structures of the native and swollen forms of cowpea chlorotic mottle virus determined by X-ray crystallography and cryo-electron microscopy. Structure **3:**63–78.
33. **Staunton, D. E., V. J. Merluzzi, R. Rothlein, R. Barton, S. D. Marlin, and T. A. Springer.** 1989. A cell adhesion molecule, ICAM-1, is the major surface receptor for rhinoviruses. Cell **56:**849–853.
34. **Xing, L., J. M. Casasnovas, and R. H. Cheng.** 2003. Structural analysis of human rhinovirus complexed with ICAM-1 reveals the dynamics of receptor-mediated virus uncoating. J. Virol. **77:**6101–6107.
35. **Xing, L., K. Tjarnlund, B. Lindqvist, G. G. Kaplan, D. Feigelstock, R. H. Cheng, and J. M. Casasnovas.** 2000. Distinct cellular receptor interactions in poliovirus and rhinoviruses. EMBO J. **19:**1207–1216.
36. **Zauner, W., D. Blaas, E. Kuechler, and E. Wagner.** 1995. Rhinovirus-mediated endosomal release of transfection complexes. J. Virol. **69:**1085–1092.